

Generated using the official AMS L^AT_EX template v6.1 two-column layout. This Work has not yet been peer-reviewed and is provided by the contributing Author(s) as a means to ensure timely dissemination of scholarly and technical Work on a noncommercial basis. Copyright and all rights therein are maintained by the Author(s) or by other copyright owners. It is understood that all persons copying this information will adhere to the terms and constraints invoked by each Author's copyright.

Köppen meets Neural Network: Revision of the Köppen Climate Classification by Neural Networks

JI LUO^a

^a School of Computing Science, Simon Fraser University

ABSTRACT: Climate change and development of data-oriented methods are appealing for new climate classification schemes. Based on the most widely used Köppen-Geiger scheme, this article proposes a neural network based climate classification method from a data science perspective. In conventional schemes, empirically handcrafted rules are used to divide climate data into climate types, resulting in certain defects. In the proposed method, a machine learning mechanism is employed to do the task. Specifically, the method first trains a convolutional neural network to fit climate data to land cover conditions, then extracts features from the trained network and finally uses a self-organizing map to cluster land pixels on the extracted features. The method is applied to cluster global land represented by 66,501 pixels (each covers 0.5 latitude degree \times 0.5 longitude degree) using 2020 land cover data and 1991-2020 climate normals, and a $4 \times 3 \times 2$ hexagonal self-organizing map clusters the land pixels into twenty-four climate types. By Kappa statistics, the obtained scheme shows good agreement with the Köppen-Geiger and Köppen-Trewartha schemes. In addition, our scheme addresses some issues of the Köppen schemes, suggests new climate types such as **As** (severe dry-wet season) and **Fw** (arctic desert), and identifies the highland group **H** without input of elevation. The proposed method is expected as an intelligent tool to monitor changes in the global climate pattern and to discover new climate types of interest that possibly emerge in the future. It may also be valuable for bio-ecology communities.

SIGNIFICANCE STATEMENT: Climate classification schemes are supposed to classify hydrothermal conditions of global land regions to indicate the formed ecosystem. The Köppen-Geiger climate classification scheme, broadly taught in high school geography class, was proposed about a century ago and is still the most widely used despite a number of defects. The reason it stands the test of time may be its relation to the ecosystem. This research fundamentally follows Köppen's original idea to map climate data to local vegetation conditions, but seeks to improve the mapping via a convolutional neural network. The result addresses some issues of the Köppen-Geiger scheme and shows the newest global climate pattern. The methodology can be helpful for both climatology and bio-ecology communities.

1. Introduction

Climate is a decisive factor of the ecosystem. The natural vegetation and human land use¹ of a region depend on key factors of the region's climate, such as the temperature, precipitation and evapotranspiration. Climate classification is introduced to describe the different climatic conditions in a categorical manner. Various world climates can be categorized into several groups and types, within each the hydrothermal conditions are similar, resulting in homogeneous land cover conditions. Hence, each climate type is

related to a certain kind of biome. This is the ecological significance marked by climate classification. In this sense, climate classification is regarded as both a descriptive tool for climate and a predictive tool for land cover, and the latter function is becoming increasingly important nowadays (Rubel and Kottek 2011).

Traditionally, the task is done via empirically handcrafting rules. Among these systems, the Köppen-Geiger climate classification, devised in the early 20th century (Köppen and Geiger 1930), is the most widely used climate classification system up to today. However, several defects of the Köppen-Geiger scheme have been reported, including fractionated subtypes (*Dsc*, *Cfc*, *Cwc*, *Csc*², etc.), disputed thresholds (0°C (Peel et al. 2007) or -3°C (Kottek et al. 2006) between *C* and *D* group, the threshold between hot and cool arid climates (Cereceda et al. 2008), etc.) and rigidity (does not scale or update its rules adapting to the changing global climate, cannot discover novel climate types (Sanderson 1999)). To address some of these deficiencies, still within the empirical framework, Trewartha (see Belda et al. 2014) modified it to create the Köppen-Trewartha scheme. In some versions of the Köppen-Geiger and Köppen-Trewartha schemes (see Cui et al. 2021), there is an *H* group denoting the highland climate, but unlike other groups, the definition is ambiguous with respect to climate variables.

Today, thanks to the advanced tools of data science and machine learning, the problem can be addressed in a more quantitative, intelligent and accurate fashion. Researchers have worked towards this direction, but many (Akrami

Corresponding author: Ji Luo, luojil@sfu.ca

¹In this article the terms *vegetation* and *land cover* are used interchangeably. The two terms do have moderately different meanings but omitting the difference comes out to be safe for our methodology.

²For clarity, Köppen-Geiger and Köppen-Trewartha types are marked in *italics* and the climate types defined by this research are in **bold**.

et al. 2022; Sathiaraj et al. 2019; Cannon 2012; Bieniek et al. 2012), clustering merely on climate variables, neglected the underlying biomes and basically deviated from Köppen's original approach. These purely unsupervised methods do not address the relation between climate and vegetation well. Recently, Metzger et al. (2013) and Gardner et al. (2020) selected physiologically relevant variables in order to embed the underlying vegetation into climate classification and did k -means clustering on those selected variables. In contrast, our research delicately designs a convolutional neural network to intelligently learn those variables itself.³ The results show the neural network performs better than manual feature selection on the large and complex global climate system and the methodology appears more natural with fewer subjective factors. For clustering, self-organizing maps (SOM) shows its advantage over k -means by emphasizing the principle components of the learned features. In terms of climate, it is able to sort the climate types by levels of humidity, temperature and continentality and produce a more structured scheme. To the best of our knowledge, the scheme derived in this research is the first data-oriented one that comprehensively considers levels of aridity, heat, evapotranspiration and precipitation pattern on a global scale. This may not be achieved without the power of neural network.

The rest of this article is organized as follows. Section 2 describes the land cover dataset and climate dataset used in this research. Section 3 explains the proposed method in detail. Section 4 reports and analyzes the intermediate results and the obtained global climate classification scheme. The final section concludes the article and discusses possible extensions and future work.

2. Dataset

This section describes the land cover dataset and climate normal dataset used in our experiment. The land cover dataset is the prediction target for the neural network while the climate normal dataset serves as the network's input. It is helpful to describe the datasets first for a better understanding of our methodology.

a. Land cover dataset

The MCD12C1 dataset (Friedl et al. 2010) of year 2020 (Antarctica excluded) was taken to construct the land cover dataset. The cover percentage of each IGBP⁴ class was used. The original dataset specifies 17 land cover types whereas some of them are considered not directly related to climate, so some types were ignored and merged, as given in Appendix A. The original resolution is $0.05^\circ \times 0.05^\circ$

³The software used in this research is MATLAB R2021b and the related toolboxes.

⁴International Geosphere-Biosphere Programme (igbp.net), closed in 2015. Most of its projects and networks have moved to Future Earth (futureearth.org).

(latitude degree \times longitude degree); I spatially aggregated it to $0.5^\circ \times 0.5^\circ$ to align with the climate normal dataset. The constructed dataset has 66,501 records, and each single record is a normalized 1×14 vector. Each vector entry stores the percentage of a certain land cover type on the $0.5^\circ \times 0.5^\circ$ land area with water or city covered area excluded. Figure 1 illustrates the calculation for a $0.5^\circ \times 0.5^\circ$ land pixel (record).

Color each $0.5^\circ \times 0.5^\circ$ land pixel with its dominating land cover type, and we get the world map of land cover as shown in Figure 2.

b. Climate normal dataset

The CRU TS v4.05 dataset (Harris et al. 2020) was used to construct the climate normal dataset. Only the *Tmp*, *Pre* and *Pet*⁵ variables are involved, namely temperature, precipitation and potential evapotranspiration. The CRU TS dataset covers global land excluding Antarctica at $0.5^\circ \times 0.5^\circ$ resolution, and the temporal granularity is one month. For each of the three variables, I averaged on each month (Jan, Feb, ..., Dec) through the years of 1991–2020, and hence a 3×12 matrix is obtained for each land pixel. The constructed dataset has 66,501 records (sea and Antarctica excluded, matching the constructed land cover dataset), and each single record is a 3×12 matrix.⁶

The datasets used in this research can be summarized as shown in Figure 3.

3. Methodology

The central component of the proposed method is a convolutional neural network which fits climate data to land cover data to create features on the co-relations between climate and land cover condition. These features are equivalent to the *physiologically relevant variables* by Metzger et al. (2013) and Gardner et al. (2020). Then a self-organizing map is used to cluster land pixels based on these features.

a. The convolutional neural network for land cover mapping

A convolutional neural network is built to predict land cover percentage by climate normals (*NN prediction* in Figure 3), as was done empirically by Köppen. The network, inspired by Köppen's empirical rules, is shown in Figure 4. It can be regarded as a spanning space for the empirical rules, and training the network is to find the best set of rules to describe the mapping between climate and land cover conditions. It is constructed of three component blocks: convolution, pooling and regression. Besides, the custom

⁵The abbreviations are used in the following sections.

⁶Of the 66,501 records, there are 46 records whose land cover vector is invalid (the whole area is lake or city). These records are not fed into neural network training, but their features are extracted by the trained network and put to clustering afterwards.

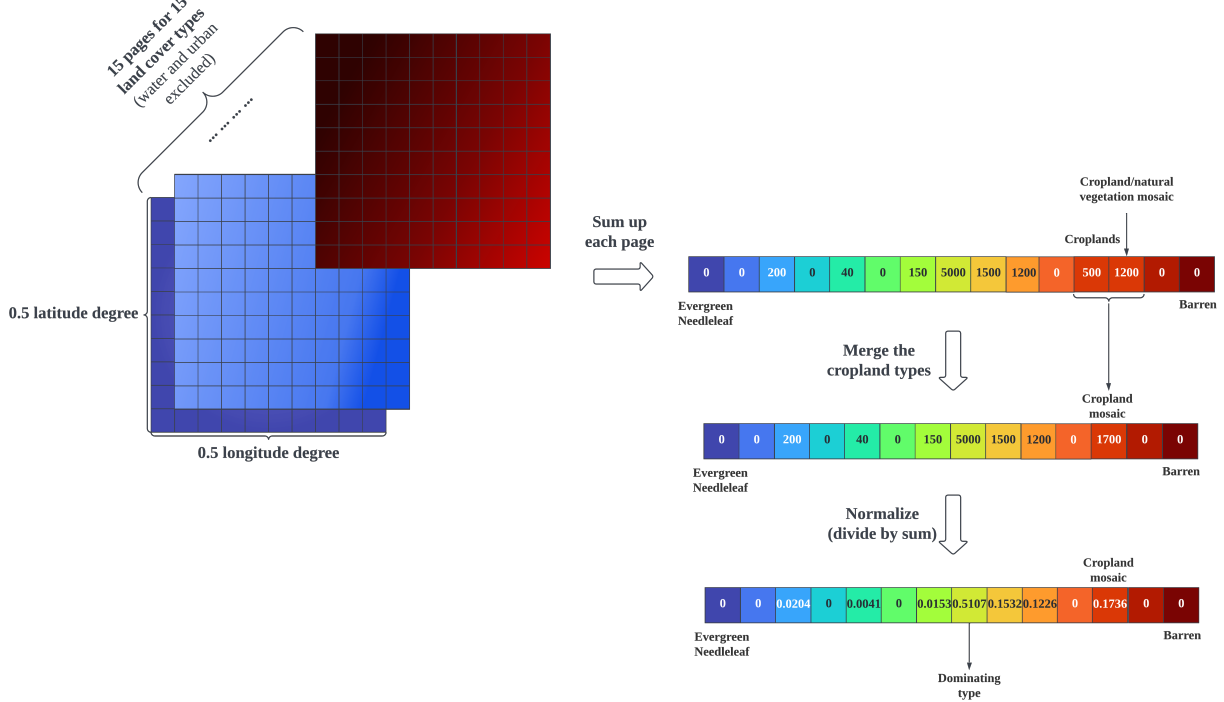


FIG. 1. Illustration of land cover data calculation. A cell on a data page stores the percentage of a land cover type on the specific $0.05^\circ \times 0.05^\circ$ area.

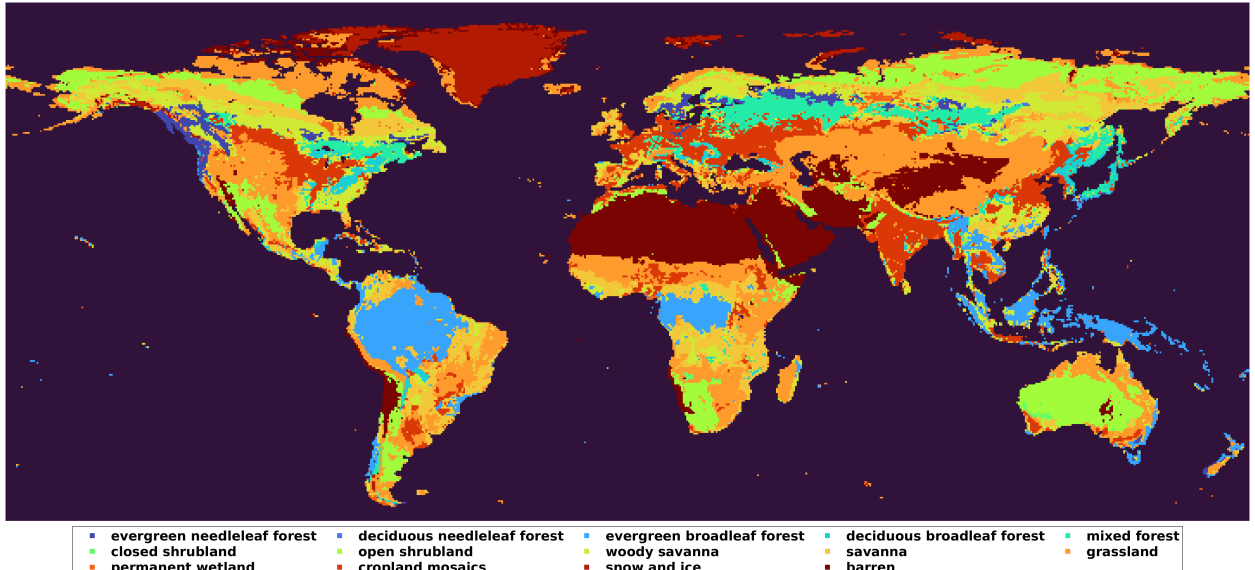


FIG. 2. World map of land cover, 2020.

activation layer is also important and will be introduced

1) THE CUSTOM ACTIVATION LAYER

The custom activation layer takes a 3×12 matrix as input and has two branches. One branch simulates em-

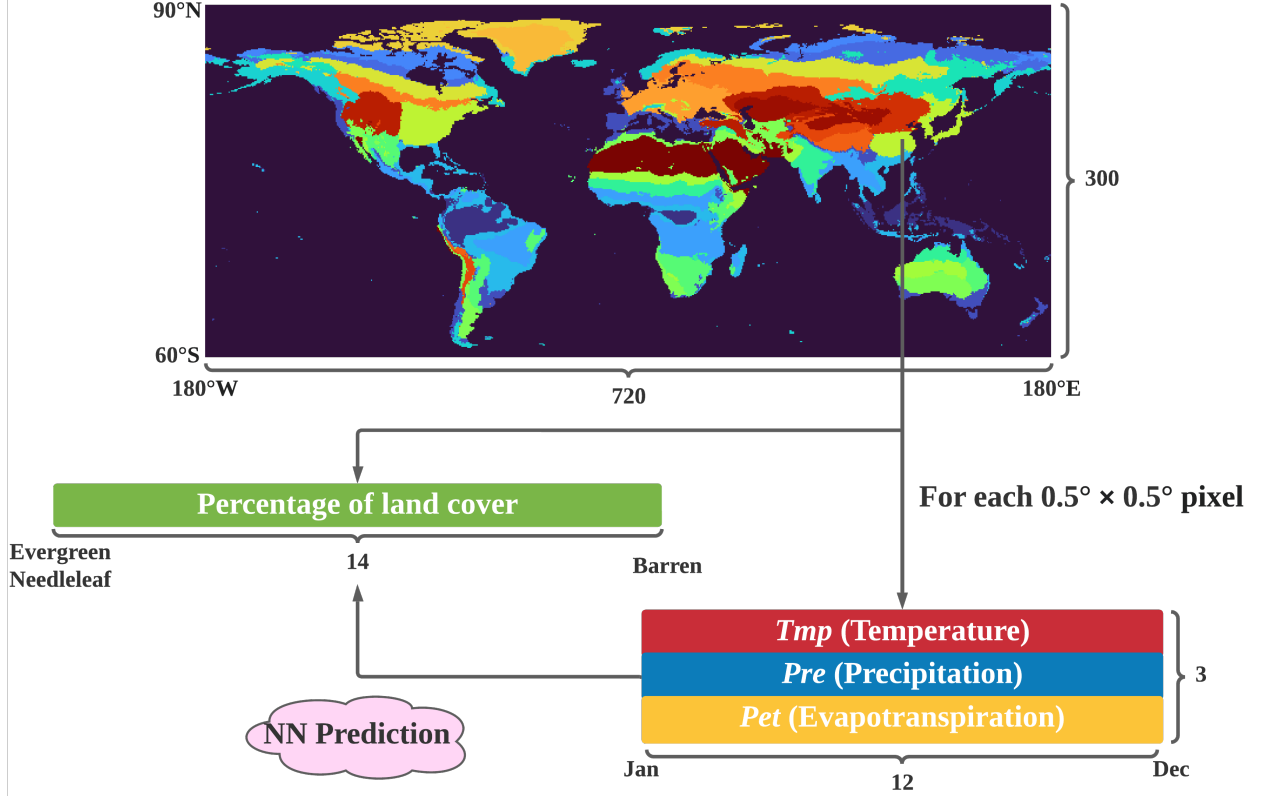


FIG. 3. Dataset structure.

pirical comparison of monthly Tmp , Pre , Pet data against certain thresholds (denoted as μ , e.g., the -3°C threshold that distinguishes between C and D groups by Köppen) by hypertangent functions:

$$y_1 = \tanh((x - \mu)/\sigma) \quad (1)$$

The other branch uses log-ReLU functions (Equation 2, Liu et al. (2019)) to learn multiplicative relationships among climate variables that exceed certain thresholds. It can derive physiologically relevant variables such as active cumulative temperature and aridity index. The two branches share the same set of thresholds for climate variables but the scaling factors σ are learned separately.

$$y_2 = \ln(\max((x - \mu)/\sigma, 0) + 1) \quad (2)$$

The workflow of this layer is shown in Figure 5. The layout of the output matrices enables interactions among climate variables of similar levels. Specifically, low levels of Tmp (standardized, e.g. $(Tmp - \mu_{t_1})/\sigma_{t_1}$) are put adjacent to low levels of Pre and Pet (standardized, e.g. $(Pre - \mu_{p_1})/\sigma_{p_1}$), and high levels of Tmp (standardized, e.g. $(Tmp - \mu_{t_4})/\sigma_{t_4}$) are put adjacent to high levels of Pre and Pet (standardized, e.g. $(Pre - \mu_{p_3})/\sigma_{p_3}$), so that

convolutions happen among similar levels. This arrangement is based on the observations that more commonly in nature Tmp , Pre , Pet are positively co-related, and that Tmp and Pre should both be high to encourage vegetation growth.

The learnable parameters involved in this layer are shown in Table 1. It is more flexible and intelligent to let the network learn these thresholds and scales on its own rather than assigning by human estimation. In addition, hypertangent activation can appear smoother than 0-1 thresholding as in empirical rules (Kalman and Kwasny 1992).

2) THE CONVOLUTION COMPONENT

The convolution component takes as input a 10×12 matrix. It consists of a circular padding layer (*cpadding*), a 2D convolution layer using 3×3 kernels (*conv*), a batch normalization layer (*batchnorm*) and two activation layers (*relu* and *tanh*), as shown in Figure 6. The layers are specified in Table 2.

The circular padding layer (Wang et al. 2018) replicates the column of January behind that of December, and vice versa. Observing the natural repetition of years, this ma-

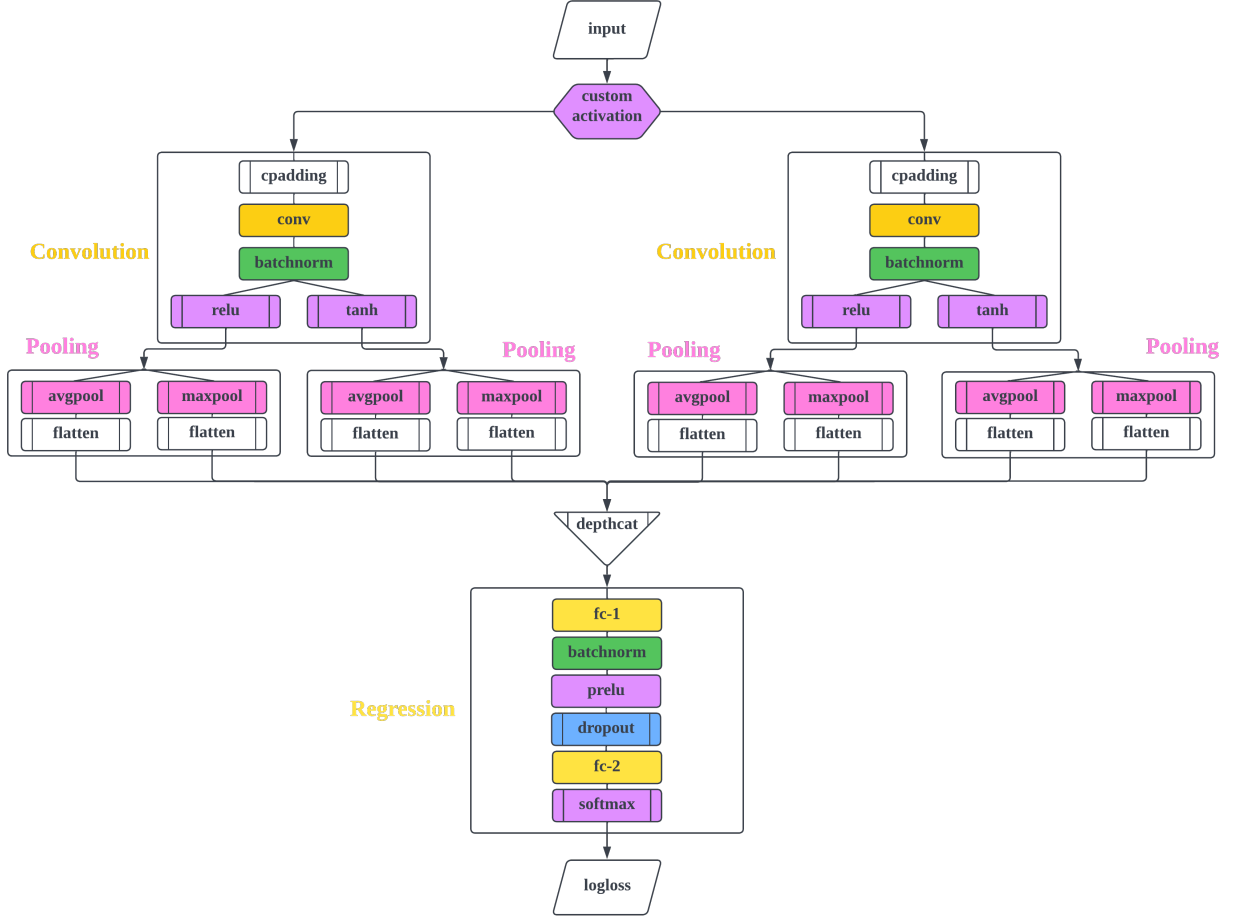


FIG. 4. Neural network structure. The layers with two vertical lines in their shape do not involve any learning; i.e., each of them represents a fixed manipulation without any learnable parameters.

TABLE 1. Learnable parameters of the custom activation layer. These parameters scale differently from other learnable parameters which are normally within $[-1, 1]$ in neural networks, so learning rate factors are specially assigned for them. The measuring unit for μ_t and σ_t is $^{\circ}\text{C}$ and for μ_p and σ_p it is millimeter (mm).

Parameter	Initial value	Learning rate factor	Description
μ_{t_1}	-18	30	For T_{mp}
μ_{t_2}	0	30	
μ_{t_3}	10	30	
μ_{t_4}	22	30	
σ_{t_i} ($1 \leq i \leq 4$)	1.5	30	For T_{mp} (hypertangent branch)
σ_{t_i} ($5 \leq i \leq 8$)	2	30	For T_{mp} (log-ReLU branch)
μ_{p_1}	10	200	For P_{re} and P_{et}
μ_{p_2}	40	200	
μ_{p_3}	100	200	
σ_{p_i} ($1 \leq i \leq 3$)	10	200	For P_{re} and P_{et} (hypertangent branch)
σ_{p_i} ($4 \leq i \leq 6$)	20	200	For P_{re} and P_{et} (log-ReLU branch)

nipulation ensures that every month is equally presented in the following convolutions.

After the *batchnorm* layer, a copy of data is made and the two copies are fed to *relu* and *tanh* respectively.

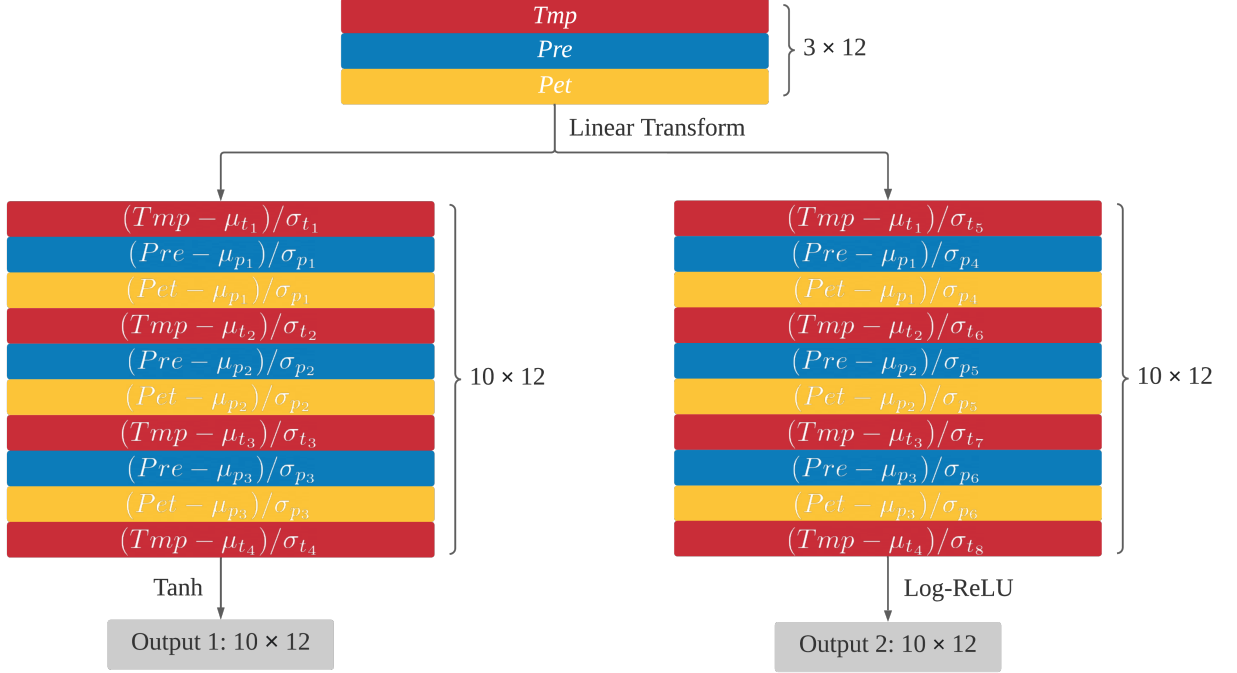


FIG. 5. Workflow of the custom activation layer.

TABLE 2. Layer specification of the convolution component. No normalization is enforced on the learnable parameters unless specified. The weights of the convolution layers are initialized as described by He et al. (2015).

Name	Description	Activations	Learnables	Learnable count
cpadding	Circular padding layer	10x14	/	0
conv	2D convolution layer with 24 3x3 kernels	8x12x24	weights 3x3x24 bias 24 (Initial value 0)	240
batchnorm	Batch normalization layer	8x12x24	offset 24 (Initial value 0) scale 24 (Initial value 1) L2 normalization factor for offset and bias: 1	48
tanh	Tanh activation layer	8x12x24	/	0
relu	ReLU activation layer	8x12x24	/	0

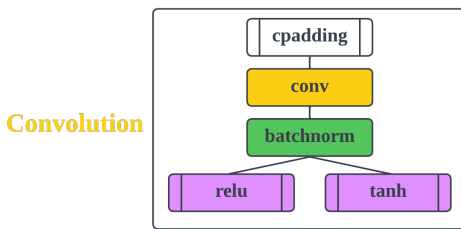


FIG. 6. The convolution component of the network.

3) THE POOLING COMPONENT

The pooling component takes a $8 \times 12 \times 24$ matrix from the convolution component and makes a copy for average

pooling and max pooling. It consists of four layers as shown in Figure 7 and the layers are specified in Table 3.

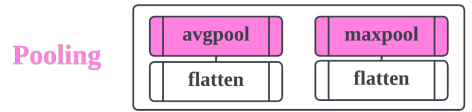


FIG. 7. The pooling component of the network.

The pooling size is 1×12 to pool across all the 12 months. By this setting, convolved 3-month features are chronologically aggregated as min/max/average statistics

over a whole year, and the season inverse between Northern and Southern Hemisphere is eliminated.

Subsequently, a concatenation layer (*depthcat*) collects output from eight pooling components to obtain 1,536 original features. Considerable duplication exists among these features so they are reduced in the following regression component.

4) THE REGRESSION COMPONENT

This component learns how the climate features are mapped to land cover conditions. The structure is given in Figure 8 and specified in Table 4. First, reduction and transformation of the original 1,536 features are done by the layer sequence of a fully connected layer (*fc-1*), a batch normalization layer (*batchnorm*) and a parametric ReLU layer (*prelu*, He et al. (2015)). The number of features is reduced half to 768 by the *fc-1* layer. A dropout layer is followed to suppress overfitting (further explanation in Section 4.a.2). Then, a fully connected layer (*fc-2*) with a softmax layer fits the 768 features to the normalized 1×14 land cover vector.

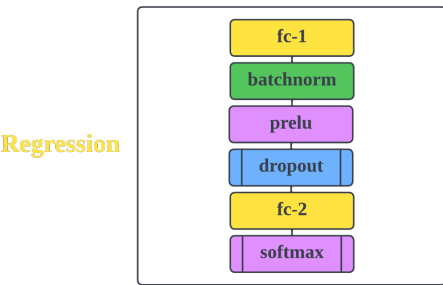


FIG. 8. The regression component of the network.

The *logloss* layer calculates error for each observation by multi-label cross entropy (Equation 3). In Equation 3, K is the number of land cover types, t_i is the truth value for the i -th type, and y_i is the predicted value. In our dataset, $K = 14$.

$$L = - \sum_{i=1}^K (t_i \ln y_i + (1 - t_i) \ln(1 - y_i)) \quad (3)$$

5) TRAINING AND FEATURE EXTRACTION

The neural network was trained using the datasets constructed of 1991–2020 climate normals (input) and land cover of 2020 (target) as specified in Section 2. The *Adam* solver (Kingma and Ba 2014) was used at initial learning rate 0.001, and it was slowed down by ten times every ten epochs in a staircase manner⁷. Other training options

followed MATLAB's default, including mini batch size as 128. The network was trained over 30 epochs. Then the climate normal dataset was again propagated through the trained network, and the activations of the *prelu* layer were fetched as observations for the next step of clustering. 66,501 observations were fetched, each consisting of 768 features.

b. SOM for climate clustering

Self-organizing maps (SOM), by Kohonen (1990), capable of capturing the structures among clusters, can be regarded as a revised version of k -means clustering. In addition to locating cluster centers in the feature space, it also manages to preserve the topology of clusters – usually cubic or hexagonal grid preset before training. Hence, unlike k -means, it would not give randomly scattered clusters. In this research a $4 \times 3 \times 2$ hexagonal grid (as shown in Figure 18) was used for climate clusters to compact the 768 features output by the *prelu* layer to 24 discrete grid points organized in a 3D space. The SOM was trained over 200 initial cover steps and 1,000 epochs in total; other settings followed MATLAB's default.

4. Results and discussion

This section will go through the experiment of our methodology on the global datasets, report and analyze the results step by step. We will look into the parameters of some important layers of the trained neural network, showcase the predicted land cover and interpret the extracted climate features and the obtained global climate classification scheme. A comparison experiment that clusters on the extracted features by k -means instead of SOM was done and the result is illustrated. Also, the obtained scheme is compared with the conventional Köppen-Geiger and Köppen-Trewartha schemes.

a. Land cover mapping

1) THE TRAINED NETWORK

In land cover mapping, the parameters of the custom activation layer and the *fc-2* layer play a key role which will be explained below.

Learned parameters of the custom activation layer are listed in Table 5. In general, the initial values preset for μ based on the Köppen rules (see Table 1) were close to the learned values. A notable observation is that σ_{p_i} ($1 \leq i \leq 3$) and σ_{p_i} ($4 \leq i \leq 6$) both significantly increase with higher precipitation level i . This means that the network learned that overabundant precipitation rarely affect the

⁷Even though the *Adam* optimizer adapts learning rates for different parameters, I still find it helpful to preset learning rates for the parameters

TABLE 3. Layer specification of the pooling component.

Name	Description	Activations	Learnables	Learnable count
avgpool	Average pooling layer Pooling size 1×12	$8 \times 1 \times 24$	/	0
maxpool	Max pooling layer Pooling size 1×12	$8 \times 1 \times 24$	/	0
flatten	Flatten layer that reshapes data to 1D	192	/	0

TABLE 4. Layer specification of the regression component. No normalization is enforced on the learnable parameters unless specified. The weights of the fully connected layers are initialized as described by He et al. (2015).

Name	Description	Activations	Learnables	Learnable count
fc-1	Fully connected layer that reduces the number of features	768	weights 768×1536 bias 768 (Initial value 0) L2 normalization factor for weights only: 2	1,180,416
batchnorm	Batch normalization layer	768	offset 768 (Initial value 0) scale 768 (Initial value 1) L2 normalization factor for offset and scale: 1	1,536
prelu	Parametric ReLU activation layer	768	alpha 768 (Initial value 0.25)	768
dropout	Dropout layer Dropout probability: 50%	768	/	0
fc-2	Fully connected layer that maps climate features to land cover conditions	14	weights 14×768 bias 14 (Initial value 0)	10,766
softmax	Softmax layer	14	/	0

vegetation so it deemed weaker discriminatory power on higher precipitation.

TABLE 5. Learned parameters of the custom activation layer.

Parameter	Initial value	Learned value
μ_{t_1}	-18	-19.1288
μ_{t_2}	0	0.2805
μ_{t_3}	10	10.0737
μ_{t_4}	22	24.2743
σ_{t_1}	1.5	3.1658
σ_{t_2}	1.5	3.4438
σ_{t_3}	1.5	1.9682
σ_{t_4}	1.5	1.8707
σ_{t_5}	2	2.0875
σ_{t_6}	2	4.4043
σ_{t_7}	2	6.0851
σ_{t_8}	2	2.0639
μ_{P_1}	10	6.6412
μ_{P_2}	40	33.5933
μ_{P_3}	100	103.3536
σ_{P_1}	10	7.3361
σ_{P_2}	10	10.3382
σ_{P_3}	10	14.8381
σ_{P_4}	20	19.0155
σ_{P_5}	20	34.9033
σ_{P_6}	20	49.2135

Learned bias parameters of the *fc-2* layer for each land cover type is listed in Table 6. It can be seen that predictions for *deciduous needleleaf forest*, *closed shrubland* and *permanent wetland* were severely suppressed by this layer. These types are relatively rare around the world. The bias parameters do not interact with the input climate data in forward propagation and thus can be seen as indicators of impact from factors other than climate on land cover. The potential natural vegetation (Hengl et al. 2018) may be obtained by setting these parameters to zero and then passing climate data again through the trained network, which is another topic for future exploration.

2) LAND COVER PREDICTION

The prediction target of the neural network is a 1×14 vector describing land cover conditions on a $0.5^\circ \times 0.5^\circ$ area (see Figure 1). Assign the land cover type with the highest cover percentage (dominating type) as the true label and similarly for the predictions given by the network, and we get the world map of predicted land cover (Figure 9) and the confusion chart (Figure 10). Figure 9 can be seen as a smoothed version of Figure 2. The predicted land cover zones appear more homogeneous in that noisy pixels are smoothed out.

From the confusion chart it can be seen that the network accurately identified land cover types such as barren and ice which are marked by pronounced climate features.

TABLE 6. Learned bias of the *fc-2* layer for each land cover type.

Land cover type	Cover percentage	Learned bias
evergreen needleleaf forest	1.84%	-0.0683
deciduous needleleaf forest	0.33%	-0.3452
evergreen broadleaf forest	6.52%	0.0638
deciduous broadleaf forest	1.70%	-0.1052
mixed forest	3.29%	0.0518
closed shrubland	0.30%	-0.3041
open shrubland	10.07%	0.0695
woody savanna	7.85%	0.0622
savanna	11.00%	0.0638
grassland	22.77%	0.0522
permanent wetland	3.97%	-0.3799
cropland mosaics	9.15%	-0.0300
snow and ice	5.62%	-0.0644
barren	15.60%	-0.0327

Types that are underrepresented or have no clear climate features, such as *closed shrubland* and *permanent wetland*, are challenging for the network (and also humans).

The prediction achieved an overall accuracy of 78.64%. The Kappa statistic κ is 0.7556, indicating very good agreement between real-world data and the prediction (Monserud and Leemans 1992). The accuracy can be bounded by the problem's nature: land cover is the result of multiple factors, including but not limited to climate, terrain topology and human activities (Zscheischler et al. 2012). Accurate prediction of a region's land cover merely by the local climate may imply overfitting. That is why the dropout layer and regularization terms were introduced to avoid overfitting.

3) EXTRACTED CLIMATE FEATURES

Climate features were extracted by propagating the climate normal dataset through the trained network and then retrieving the activations of the *prelu* layer.

The *prelu* layer derived 768 climate features for clustering. It is not feasible to analyze them one by one, so principle component analysis (PCA) was applied first. Out of the 768 components after PCA, 428 components explained over 99% of the information. The most prominent three components are depicted in Figure 11.

With the explaining proportion decreasing, the climatological or biophysiological meanings of the features become more obscure and harder to interpret. Still from the three illustrated, we can see that the network did learn a lot of informative features for land cover prediction.

b. Climate clustering

1) GENERAL

The $4 \times 3 \times 2$ hexagonal SOM gives 24 climate types, as shown in Table 7 and Figure 12. Naming conventions

basically follow the Köppen scheme. The first letter mainly focuses on temperature zone and the second letter describes the precipitation pattern. The covering region map and representative climate chart of each climate type are given in the supplementary materials.

It is worth noting here that our methodology successfully identified the highland group **H** even though no altitude data was presented to the network. This could be explained by the network's capturing the exceptionally high evapotranspiration combined with low temperature which is a unique feature of highland.

2) COMPARISON WITH *k*-MEANS CLUSTERING

For comparison, *k*-means clustering was also conducted on the extracted features. Parameters customized for MATLAB *kmeans* function: $k = 24$ and *OnlinePhase* to be *on*. The result is shown in Figure 13.

It can be seen the result of SOM (Figure 12) is more preferable. *k*-means clustering may not focus on the principle components of features and can fall for the extremely high dimensionality.

3) COMPARISON WITH THE KÖPPEN-GEIGER SCHEME

The Köppen-Geiger scheme used for comparison here is defined in Appendix B.

To calculate the Kappa statistic between the proposed scheme and the Köppen-Geiger scheme, a mapping between types is needed. We intuitively make a mapping as shown in Figure 14. Then, the confusion chart between the two schemes can be given as in Figure 15 and the Kappa statistic κ is figured out to be 0.5620. This value indicates good agreement between our scheme and the Köppen-Geiger scheme by the standard stated by Monserud and Leemans (1992).

On top of agreement, the most important improvement of our scheme is that it groups the fractionated and unorganized subarctic types (*Dfc*, *Dwc*, *Dsc*, *Dfd*, *Dwd*, *Cfc*, *Cwc*, *Csc*, part of *ET*) into organized groups (**E** and **H**). Secondly, the arid group **B** is finer: **BSh** mainly goes into two types, **As** which has a brief warm and humid season, and **Cs** where mild to moderate aridity persists throughout the year; **Bh** is distinguished from **Bs** (*BWh*) by its milder aridity (the dominating vegetation is shrubland rather than desert); **Bk** is split out to hold the foggy and cool dry climate sometimes referred as *BWn* or *BSn* (Cereceda et al. 2008). In the arctic zone, the **Fw** type is proposed to distinguish barren land from ice sheet.

Generally, our scheme pays more attention to the arid and cold zones compared with conventional schemes. This is because in our dataset, every land pixel has equal weight, while in schemes by human experts, naturally, densely human-populated areas gain more focus. This can be unfair. For example, it is commonly acknowledged that global warming is more pronounced in the arctic regions

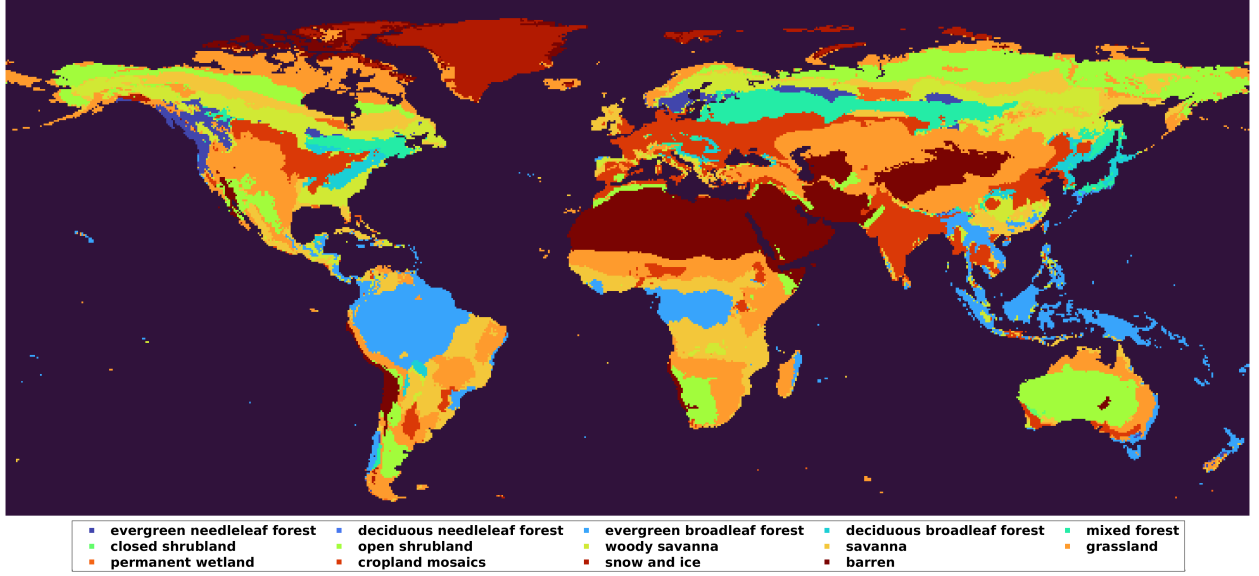


FIG. 9. World map of predicted land cover by 1991–2020 climate normals. Color scheme same as Figure 2.

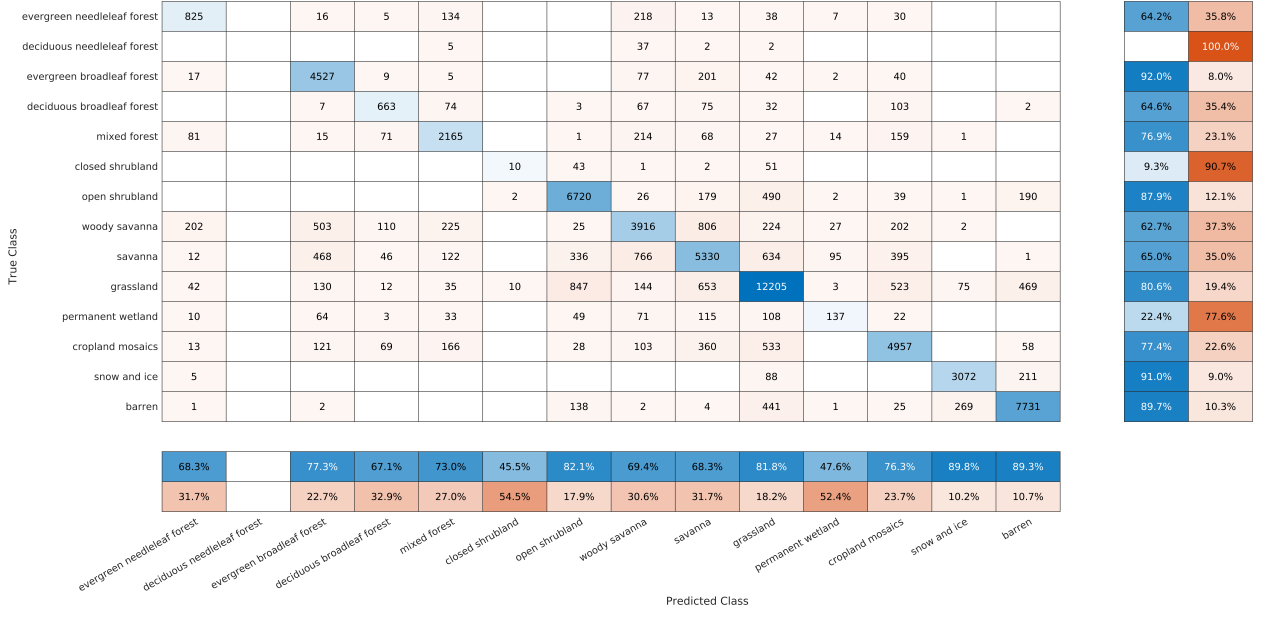


FIG. 10. Confusion chart of land cover prediction.

and the acceleration of ice melting there can be disruptive for global climate (Lee 2014). The equal treatment of global land regions is valuable to draw more attention on the vulnerable zones underrepresented by conventional climate classification schemes.

There are no individual Mediterranean climate types (*Csa*, *Csb*, *Dsa*, *Dsb*) in the derived scheme. This can be attributed to the lack of representative Mediterranean

vegetation types (e.g. sclerophyll) in the land cover dataset. Whether or not this is desirable is yet to be discussed.

4) COMPARISON WITH THE KÖPPEN-TREWARTHA SCHEME

The Köppen-Trewartha scheme used for comparison here is defined in Appendix C.

Similarly, a mapping between the proposed scheme and the Köppen-Trewartha scheme is made as shown in Figure 16 and the confusion chart is shown in Figure 17.

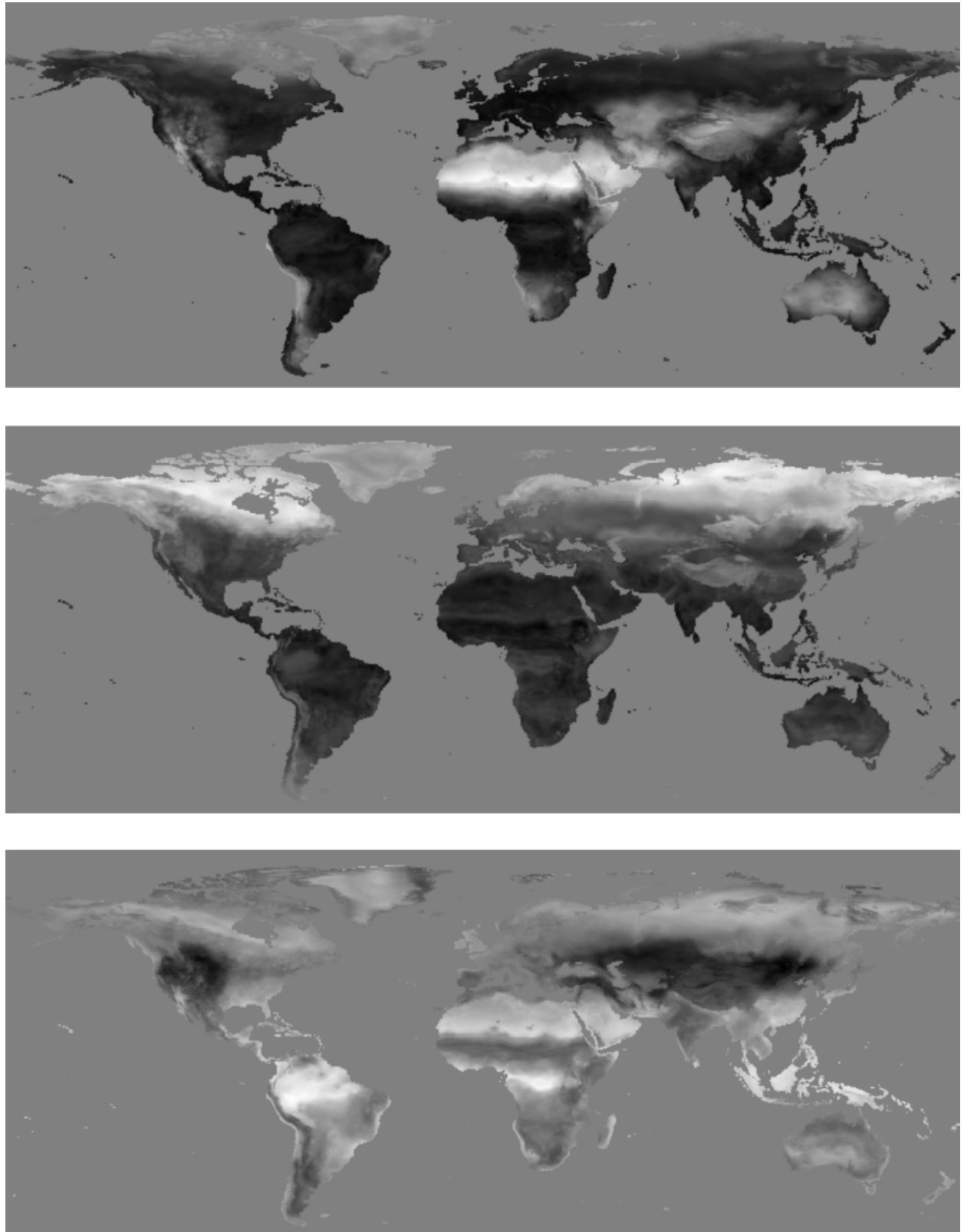


FIG. 11. Three principle components extracted by the network. Brighter regions mean higher values. From top to bottom, feature 1, explaining 13.37% of information, implies aridity. Feature 2, explaining 8.23%, can be regarded as subarctic index. Feature 3, explaining 5.94%, is inversely linked to continentality.

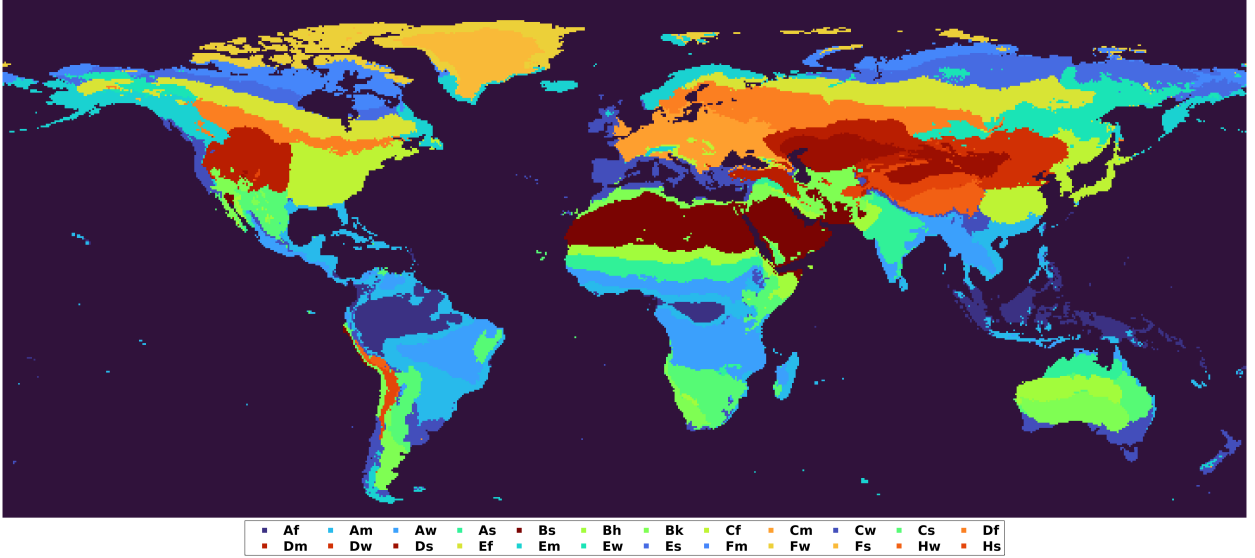
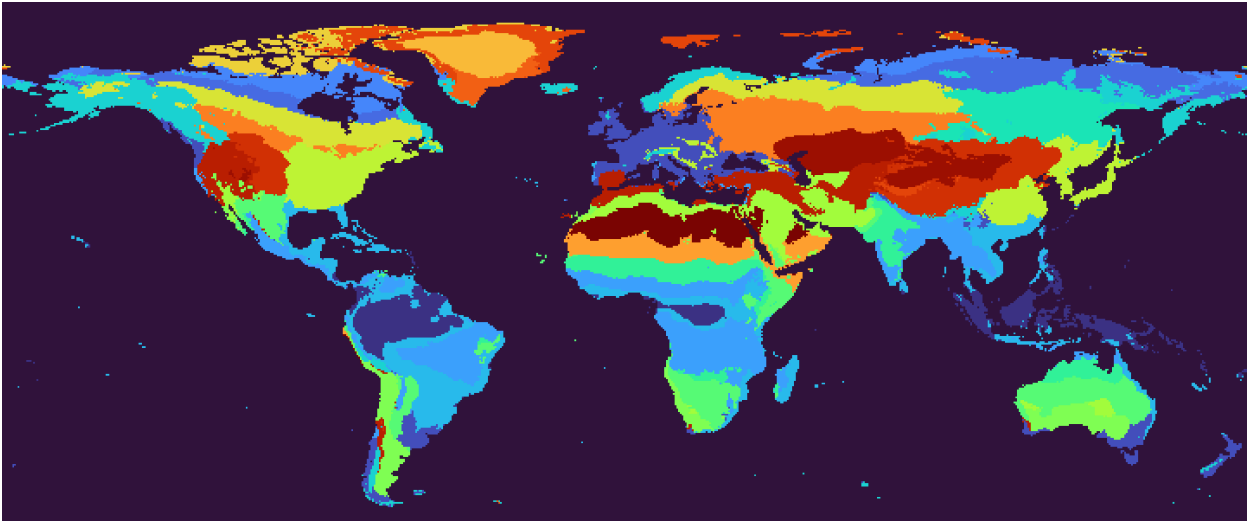


FIG. 12. World map of the climate clustering result.

TABLE 7. Climate types specification. Besides there are the **B** (dry with high temperature) group: **Bs** (hot desert), **Bh** (hot dry), **Bk** (warm dry), and the **H** (highland) group: **Hw** (highland monsoonal), **Hs** (dry highland).

	A	C	D	E	F
	warm with humid season	temperate	continental	subarctic	arctic
f	Af	Cf	Df	Ef	/
abundant precipitation	rainforest	humid temperate	humid continental	humid subarctic	
m	Am	Cm	Dm	Em	Fm
moderate/maritime	warm humid	temperate oceanic	moderate continental	subarctic oceanic	tundra
w	Aw	Cw	Dw	Ew	Fw
dry-wet season	warm dry-wet season	temperate dry-wet season	continental monsoonal	subarctic monsoonal	arctic desert
s	As	Cs	Ds	Es	Fs
severe/dry	severe dry-wet season	dry temperate	dry continental	severe subarctic	icecap

FIG. 13. World map of the *k*-means clustering result. Comparing with the result of SOM (Figure 12), the highland group is not identified and the extreme climate types (arctic and hot desert) are overly fractionated.

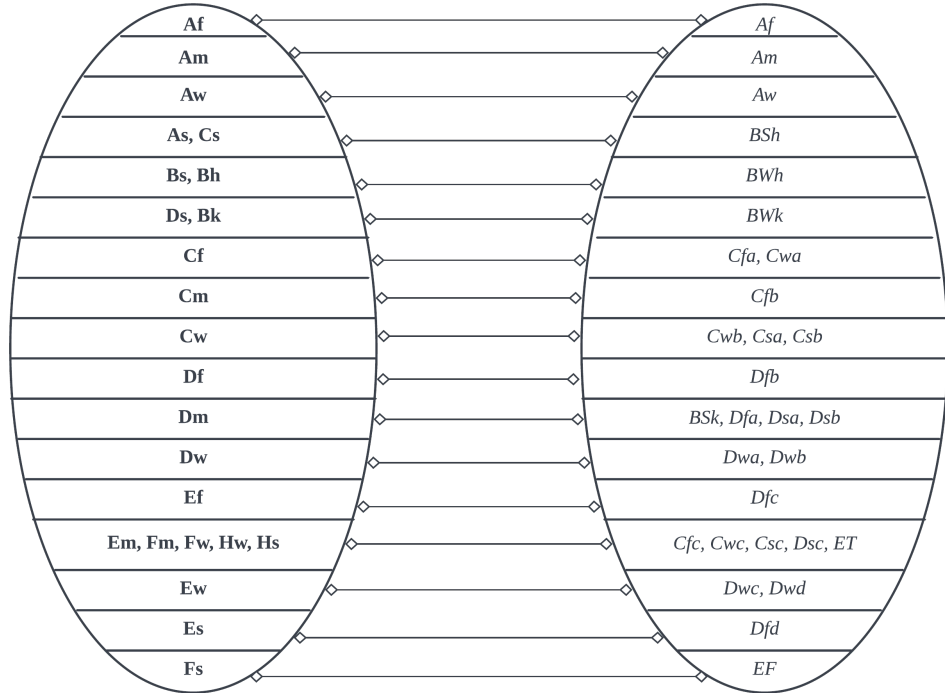


FIG. 14. A mapping between our scheme and the Köppen-Geiger scheme.

FIG. 15. Confusion chart between our scheme and the Köppen-Geiger scheme. Labels on the bottom are Köppen-Geiger types and labels on the left are our types.

The Kappa statistic κ is figured out to be 0.6800, indicating good agreement between our scheme and the Köppen-Trewartha scheme by the standard stated by Monserud and Leemans (1992).

The Köppen-Trewartha scheme and our scheme have largely different views on the division of mid-latitude temperate climates (*Cf*, *Cs*, *Do*, *Dc* / **Cf**, **Cm**, **Cw**, **Df**) hence we may not figure out a finer mapping between these

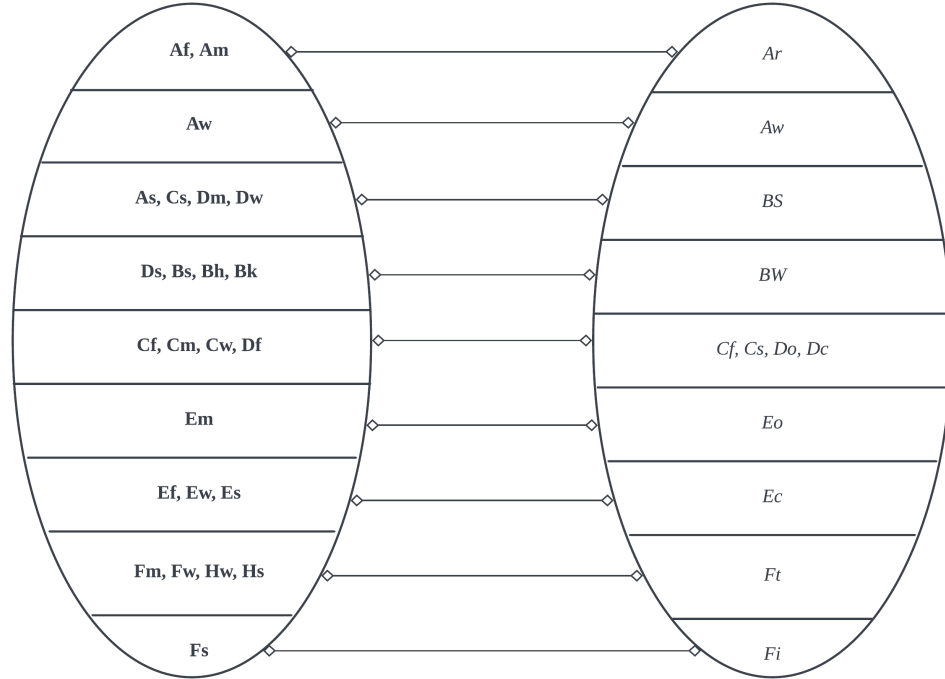


FIG. 16. A mapping between our scheme and the Köppen-Trewartha scheme.

Af,Am	3944	105	2059	1083					
As,Cs,Dm,Dw		6356	381	507	2023	165	30		
Aw	12	810	3364	563					
Cf,Cm,Cw,Df		2419	9	7957	231	934	220	9	
Ds,Bs,Bh,Bk		95	12	244	10437				
Ef,Ew,Es		808		323	32	8912	5	363	
Em		174		229	2	1224	728	749	
Fm,Fw,Hw,Hs		848		93	452	605	87	4912	299
Fs								126	1561
	Ar	BS	Aw	Cf,Cs,Do,Dc	BW	Ec	Eo	Ft	Fi

FIG. 17. Confusion chart between our scheme and the Köppen-Trewartha scheme. Labels on the bottom are Köppen-Trewartha types and labels on the left are our types.

types. Agreement with the Köppen-Trewartha scheme is better than Köppen-Geiger mainly because the Köppen-Trewartha scheme has a well-defined subarctic group and there are fewer types.

5) STRUCTURE OF THE CLIMATE TYPES

Further investigation of the proposed climate classification scheme can be conducted in terms of the hierarchical and grid structures of the climate types, as shown in the

grid chart of Figure 18 and the dendrogram of Figure 19. These structures show that the climate types are basically well organized, which is the merit of SOM.

5. Conclusion and future work

While the climatological and ecological validity and significance of this scheme need to be studied further, as the brief analysis in Section 4 shows, the proposed neural network approach of climate clustering shows a good fit to real-world land cover and appears more natural than empirical climate classification schemes. With the derived scheme, for any specific place, given its monthly series of temperature, precipitation and potential evapotranspiration, its climate type can be figured out by passing the series (a 3×12 matrix) through the trained network, retrieving the activations of the *prelu* layer and finding the nearest neighbor among the obtained twenty-four cluster centers.

The clustering result is actually not the central focus of this article as global climate pattern may change over time.

However, no matter how it changes, the proposed method can always adapt to it and detect these changes. This is the essence of this method to outperform any empirical ones.

The method may also be applied to a smaller region like a country or a province for a fine climate classification of that specific area. Also, the definition of land cover types can vary, guiding the neural network to focus on physiologically relevant variables that are important for certain biomes, for example the Mediterranean biome. As discussed in Section 4.b.3, on the land cover dataset marked with such biomes, our method is expected to identify Mediterranean climate types. Another revision can be made in the broad *cropland mosaics* type. For instance, rice cropland and wheat cropland are featured by literally different climate conditions; a further division of the type may help. Seeing this, the proposed neural network may also be used to investigate the climate conditions favored by certain biospecies. It is expected that the proposed neural network and analysis of the extracted features are found to be a useful toolbox bridging the climatology and bio-ecology communities.

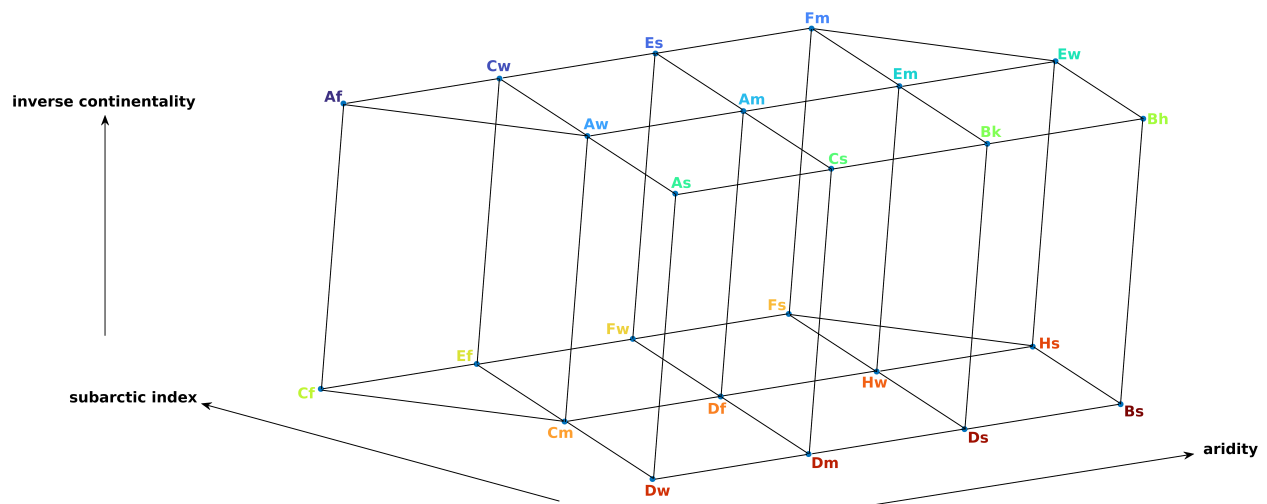


FIG. 18. Grid chart of climate types. It illustrates the SOM topology, where the three axes are roughly in accordance with the three principle components of the features in Section 4.a.3.

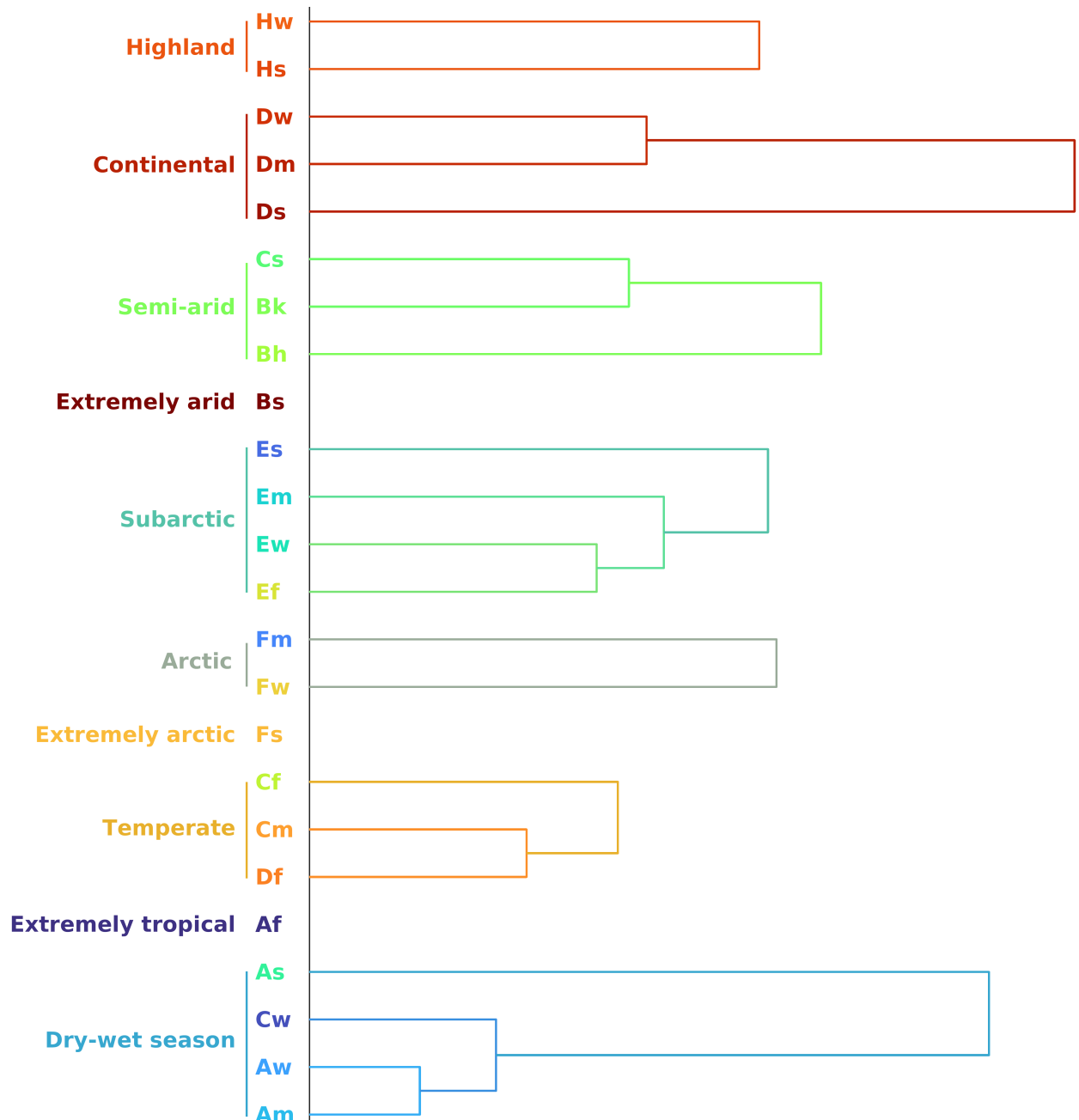


FIG. 19. Dendrogram of climate types. It is a hierarchical clustering tree using Ward's linkage plotted by recursively grouping two closest (most similar) climate types into one, and the horizontal length of the connecting line is negatively related to the similarity between the two connected clusters. High-level connecting lines are omitted.

Acknowledgments. Thank SFU for the MATLAB license which facilitates the scientific computing in this research. I kindly appreciate Land Processes Distributed Active Archive Center (LP DAAC), UK's Natural Environment Research Council (NERC) and the US Department of Energy who make the land cover and climate dataset publicly available. I used the MATLAB *kappa* function by Cardillo (<https://www.mathworks.com/matlabcentral/fileexchange/15365>) to calculate the Kappa statistics.

Data availability statement. MCD12C1 data are available through <http://lpdaac.usgs.gov/products/mcd12c1v006>. CRU TS data are available through <http://crudata.uea.ac.uk/cru/data/hrg>. MATLAB data, code and details of the climate types are supplementary materials available at <https://github.com/slclju/nn-climate-classification>. The neural network was also implemented in Python/Tensorflow (see <https://github.com/slclju/nn-climate-classification-py>), but the result is not as good as MATLAB's.

APPENDIX A

Specification of land cover types

See Table A1 (Sulla-Menashe and Friedl 2018). *Crop-lands* and *Cropland/Natural Vegetation Mosaics* were merged into one single type.

APPENDIX B

Specification of the Köppen-Geiger climate classification

Table B1 specifies the version of Köppen-Geiger climate classification (Belda et al. 2014) used in this research. In the table,

TAP is short for total annual precipitation,

MAT is short for mean annual temperature,

T means the average temperature of each month,

P means the precipitation of each month,

T_{hot} means the average temperature of the hottest month, similarly for *T_{cold}*,

P_{dry} stands for the lowest monthly precipitation,

P_{summer,wet} measures the highest monthly precipitation in the hottest three months, similarly for *P_{summer,dry}*, *P_{winter,wet}* and *P_{winter,dry}*,

P_{thresh} is the threshold for arid climates. Its baseline is $20MAT$. If the precipitation in the warmest six months constitute over 70% of annual precipitation, then 280 is added to the baseline; if the percentage is between 30% and 70%, then 140 is added.

Potential evapotranspiration is not explicitly involved in the scheme.

Apply these rules on our climate normal dataset, and we get the world's Köppen-Geiger climate classification map based on 1991-2020 climate normals of $0.5^\circ \times 0.5^\circ$ resolution as shown in Figure B1.

APPENDIX C

Specification of the Köppen-Trewartha climate classification

Table C1 specifies the version of Köppen-Trewartha climate classification (Belda et al. 2014) used in this research. In the table,

TAP is short for total annual precipitation,

T means the average temperature of each month,

P means the precipitation of each month,

T_{hot} means the average temperature of the hottest month, similarly for *T_{cold}*,

P_{summer,dry} measures the lowest monthly precipitation in the hottest three months, similarly for *P_{winter,wet}*,

P_{thresh} is the threshold for arid climates. $P_{thresh} = 23MAT - 6.4r + 410$, where *MAT* is the mean annual temperature, *r* is the proportion of precipitation in the coldest six months against *TAP*.

Potential evapotranspiration is not explicitly involved in the scheme.

Apply these rules on our climate normal dataset, and we get the world's Köppen-Trewartha climate classification map based on 1991-2020 climate normals of $0.5^\circ \times 0.5^\circ$ resolution as shown in Figure C1.

TABLE A1. Land cover type specification. In the third column a slash denotes the land cover type is ignored since it is not land or not directly related to climate.

Name in MCD12C1	Description	Name in the constructed dataset
Water Bodies	At least 60% of area is covered by permanent water bodies.	/
Evergreen Needleleaf Forests	Dominated by evergreen conifer trees (canopy > 2m). Tree cover > 60%.	evergreen needleleaf forest
Evergreen Broadleaf Forests	Dominated by evergreen broadleaf and palmate trees (canopy > 2m). Tree cover > 60%.	evergreen broadleaf forest
Deciduous Needleleaf Forests	Dominated by deciduous needleleaf (larch) trees (canopy > 2m). Tree cover > 60%.	deciduous needleleaf forest
Deciduous Broadleaf Forests	Dominated by deciduous broadleaf trees (canopy > 2m). Tree cover > 60%.	deciduous broadleaf forest
Mixed Forests	Dominated by neither deciduous nor evergreen (40 - 60% of each) tree type (canopy > 2m). Tree cover > 60%.	mixed forest
Closed Shrublands	Dominated by woody perennials (1 - 2m height) > 60% cover.	closed shrubland
Open Shrublands	Dominated by woody perennials (1 - 2m height) 10 - 60% cover.	open shrubland
Woody Savannas	Tree cover 30 - 60% (canopy > 2m).	woody savanna
Savannas	Tree cover 10 - 30% (canopy > 2m).	savanna
Grasslands	Dominated by herbaceous annuals (< 2m).	grassland
Permanent Wetlands	Permanently inundated lands with 30 - 60% water cover and > 10% vegetated cover.	permanent wetland
Croplands	At least 60% of area is cultivated cropland.	cropland mosaics
Cropland/Natural Vegetation Mosaics	Mosaics of small-scale cultivation 40 - 60% with natural tree, shrub, or herbaceous vegetation.	
Urban and Built-up Lands	At least 30% impervious surface area including building materials, asphalt, and vehicles.	/
Permanent Snow and Ice	At least 60% of area is covered by snow and ice for at least 10 months of the year.	snow and ice
Barren	At least 60% of area is non-vegetated barren (sand, rock, soil) areas with less than 10% vegetation.	barren

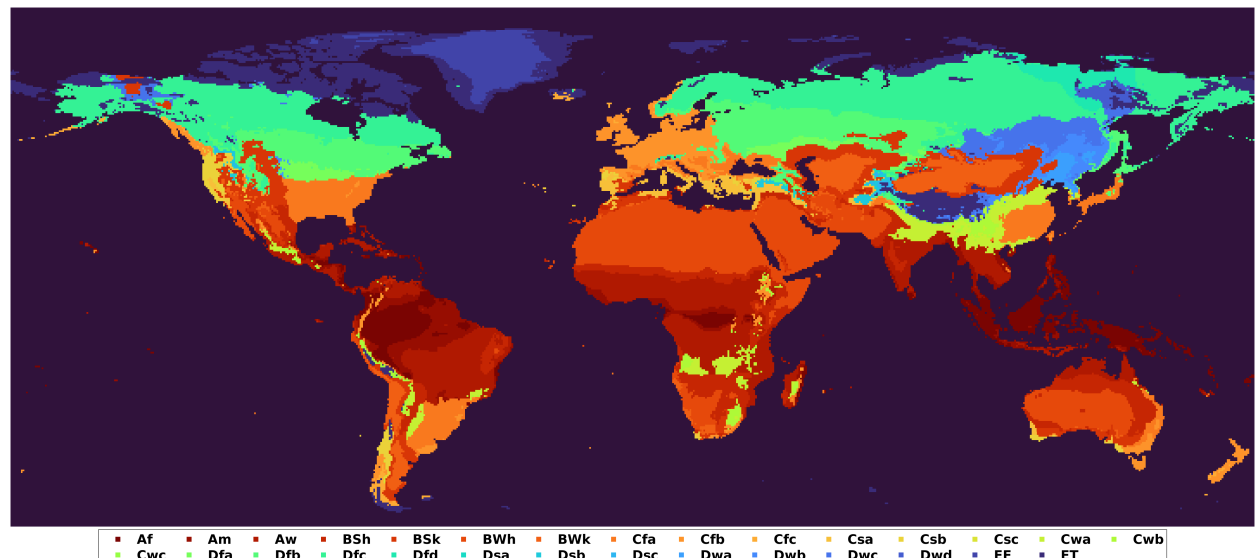


FIG. B1. World map of Köppen-Geiger climate classification, 1991-2020.

TABLE B1. Specification of the Köppen-Geiger climate types. The measuring units for precipitation and temperature are millimeter (mm) and °C, respectively. Commas in the criteria mean logical and.

Main Group	Group	Subgroup	Criteria
<i>B</i> arid			$TAP < P_{thresh}$
	<i>W</i> extremely arid/desert		$TAP < P_{thresh}/2$
	<i>S</i> semi-arid/steppe		not <i>W</i>
		<i>k</i> cool	$MAT < 18$
		<i>h</i> hot	not <i>k</i>
<i>A</i> tropical			$T_{cold} \geq 18$
	<i>f</i> rainforest		$P_{dry} \geq 60$
	<i>w</i> dry-wet season/savanna		not <i>f</i> , $P_{dry} < 100 - TAP/25$
	<i>m</i> monsoonal		neither <i>f</i> nor <i>w</i>
<i>E</i> arctic			$T_{hot} < 10$
	<i>F</i> icecap		$T_{hot} < 0$
	<i>T</i> tundra		not <i>F</i>
<i>C</i> temperate			$T_{cold} > -3$
<i>D</i> continental			not <i>C</i>
	<i>w</i> monsoonal		$P_{summer,wet} > 10P_{winter,dry}$
	<i>s</i> Mediterranean		$P_{winter,wet} > 3P_{summer,dry}$, $P_{summer,dry} < 30$
	<i>f</i> constantly humid		neither <i>w</i> nor <i>s</i>
		<i>c</i> subarctic	$count(T > 10) < 4$
		<i>d</i> extreme winter	in <i>c</i> , $T_{cold} \leq -38$
		<i>a</i> hot summer	$T_{hot} > 22$
		<i>b</i> cool summer	neither <i>c</i> nor <i>a</i>

TABLE C1. Specification of the Köppen-Trewartha climate types. The measuring units for precipitation and temperature are millimeter (mm) and °C, respectively. Commas in the criteria mean logical and.

Main Group	Group	Criteria
<i>B</i> arid		$TAP < P_{thresh}$
	<i>W</i> extremely arid/desert	$TAP < P_{thresh}/2$
	<i>S</i> semi-arid/steppe	not <i>W</i>
<i>A</i> tropical		$T_{cold} \geq 18$
	<i>r</i> rainforest	$count(P \geq 60) \geq 10$
	<i>w</i> dry-wet season/savanna	not <i>r</i>
<i>F</i> arctic		$T_{hot} < 10$
	<i>i</i> icecap	$T_{hot} < 0$
	<i>t</i> tundra	not <i>i</i>
<i>C</i> subtropical		$count(T > 10) \geq 8$
	<i>s</i> Mediterranean	$TAP < 890$, $P_{winter,wet} > 3P_{summer,dry}$, $P_{summer,dry} < 30$
	<i>f</i> humid	not <i>s</i>
<i>D</i> temperate		$count(T > 10) \geq 4$
	<i>c</i> continental	$T_{cold} < 0$
	<i>o</i> oceanic	not <i>c</i>
<i>E</i> subarctic		not <i>D</i>
	<i>c</i> continental	$T_{cold} < 0$
	<i>o</i> oceanic	not <i>c</i>

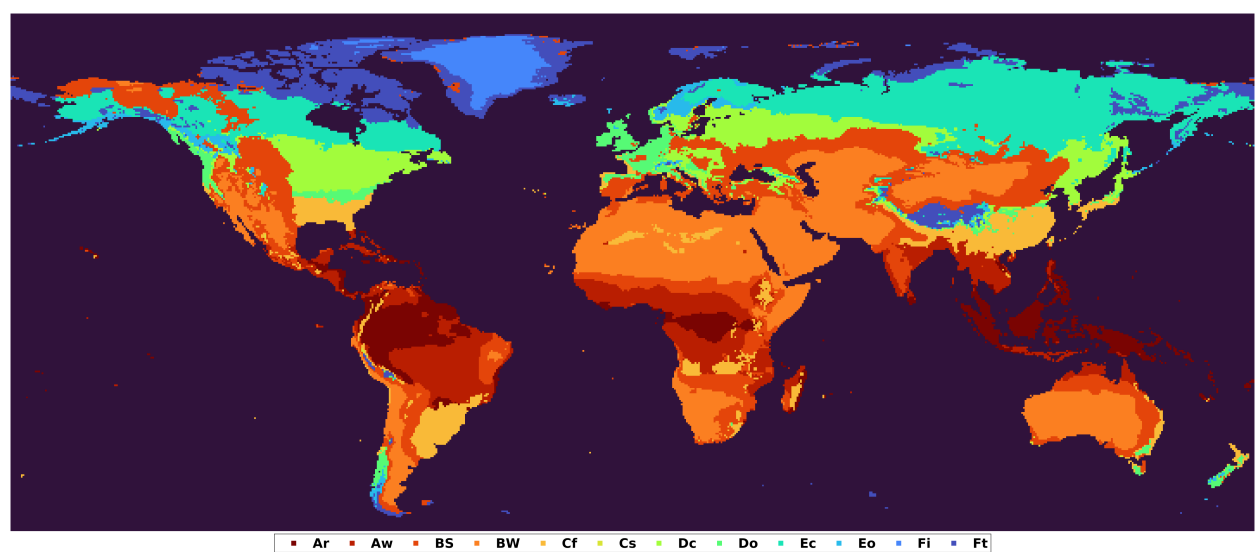


FIG. C1. World map of Köppen-Trewartha climate classification, 1991-2020.

References

- Akrami, N., K. Ziarati, and S. Dev, 2022: Graph-based local climate classification in Iran. *International Journal of Climatology*, **42** (3), 1337–1353.
- Belda, M., E. Holtanová, T. Halenka, and J. Kalvová, 2014: Climate classification revisited: from Köppen to Trewartha. *Climate research*, **59** (1), 1–13.
- Bieniek, P. A., and Coauthors, 2012: Climate divisions for Alaska based on objective methods. *Journal of Applied Meteorology and Climatology*, **51** (7), 1276–1289.
- Cannon, A., 2012: Köppen versus the computer: Comparing Köppen-Geiger and multivariate regression tree climate classifications in terms of climate homogeneity. *Hydrology and Earth System Sciences*, **16** (1), 217–229.
- Cereceda, P., H. Larraín, P. Osses, M. Farías, and I. Egaña, 2008: The climate of the coast and fog zone in the Tarapacá region, Atacama Desert, Chile. *Atmospheric Research*, **87** (3-4), 301–311.
- Cui, D., S. Liang, and D. Wang, 2021: Observed and projected changes in global climate zones based on Köppen climate classification. *Wiley Interdisciplinary Reviews: Climate Change*, **12** (3), e701.
- Friedl, M. A., D. Sulla-Menashe, B. Tan, A. Schneider, N. Ramankutty, A. Sibley, and X. Huang, 2010: MODIS collection 5 global land cover: Algorithm refinements and characterization of new datasets. *Remote Sensing of Environment*, **114** (1), 168–182.
- Gardner, A. S., I. M. Maclean, and K. J. Gaston, 2020: A new system to classify global climate zones based on plant physiology and using high temporal resolution climate data. *Journal of Biogeography*, **47** (10), 2091–2101.
- Harris, I., T. J. Osborn, P. Jones, and D. Lister, 2020: Version 4 of the CRU TS monthly high-resolution gridded multivariate climate dataset. *Scientific Data*, **7** (1), 1–18.
- He, K., X. Zhang, S. Ren, and J. Sun, 2015: Delving deep into rectifiers: Surpassing human-level performance on Imagenet classification. *Proceedings of the IEEE International Conference on Computer Vision*, 1026–1034.
- Hengl, T., M. G. Walsh, J. Sanderman, I. Wheeler, S. P. Harrison, and I. C. Prentice, 2018: Global mapping of potential natural vegetation: an assessment of machine learning algorithms for estimating land potential. *PeerJ - Life and Environment*, **6**, e5457.
- Kalman, B. L., and S. C. Kwasny, 1992: Why tanh: choosing a sigmoidal function. *[Proceedings 1992] IJCNN International Joint Conference on Neural Networks*, IEEE, Vol. 4, 578–581.
- Kingma, D. P., and J. Ba, 2014: Adam: A method for stochastic optimization. *arXiv preprint arXiv:1412.6980*.
- Kohonen, T., 1990: The self-organizing map. *Proceedings of the IEEE*, **78** (9), 1464–1480.
- Köppen, W., and R. Geiger, 1930: *Handbuch der klimatologie*, Vol. 1. Gebrüder Borntraeger Berlin.
- Kottek, M., J. Grieser, C. Beck, B. Rudolf, and F. Rubel, 2006: World map of the Köppen-Geiger climate classification updated.
- Lee, S., 2014: A theory for polar amplification from a general circulation perspective. *Asia-Pacific Journal of Atmospheric Sciences*, **50** (1), 31–43.
- Liu, Y., J. Zhang, C. Gao, J. Qu, and L. Ji, 2019: Natural-logarithm-rectified activation function in convolutional neural networks. *2019 IEEE 5th International Conference on Computer and Communications (ICCC)*, IEEE, 2000–2008.
- Metzger, M. J., R. G. Bunce, R. H. Jongman, R. Sayre, A. Trabucco, and R. Zomer, 2013: A high-resolution bioclimate map of the world: a unifying framework for global biodiversity research and monitoring. *Global Ecology and Biogeography*, **22** (5), 630–638.
- Monserud, R. A., and R. Leemans, 1992: Comparing global vegetation maps with the Kappa statistic. *Ecological Modelling*, **62** (4), 275–293.
- Peel, M. C., B. L. Finlayson, and T. A. McMahon, 2007: Updated world map of the Köppen-Geiger climate classification. *Hydrology and Earth System Sciences*, **11** (5), 1633–1644.
- Rubel, F., and M. Kottek, 2011: Comments on: "the thermal zones of the earth" by Wladimir Köppen (1884). *Meteorologische Zeitschrift*, **20** (3), 361.
- Sanderson, M., 1999: The classification of climates from Pythagoras to Köppen. *Bulletin of the American Meteorological Society*, **80** (4), 669–674.
- Sathiaraj, D., X. Huang, and J. Chen, 2019: Predicting climate types for the Continental United States using unsupervised clustering techniques. *Environmetrics*, **30** (4), e2524.
- Sulla-Menashe, D., and M. A. Friedl, 2018: User guide to collection 6 MODIS land cover (MCD12Q1 and MCD12C1) product. *USGS: Reston, VA, USA*, **1**, 18.
- Wang, T.-H., H.-J. Huang, J.-T. Lin, C.-W. Hu, K.-H. Zeng, and M. Sun, 2018: Omnidirectional CNN for visual place recognition and navigation. *2018 IEEE International Conference on Robotics and Automation (ICRA)*, IEEE, 2341–2348.
- Zscheischler, J., M. D. Mahecha, and S. Harmeling, 2012: Climate classifications: the value of unsupervised clustering. *Procedia Computer Science*, **9**, 897–906.